ACS OMEGA

Open Access

http://pubs.acs.org/journal/acsodf

Article

Research on Gas-Assisted Extrusion of Elastic Material Round-Tube for Flexible Robot Body

Shiyu Jiang, Yimeng Yu, Songtao Wang,* Liling Zhang,* Zhong Yu, and Zhi Shen

Cite This: *ACS Omega* 2024, 9, 25996−26003

Read Online

ACCESS | Metrics & More | Article Recommendations

ABSTRACT: The flexible robot is widely used in a variety of fields such as medical treatment, rescue and disaster relief, industry, and agriculture. Using elastic materials to prepare flexible robot body structures is the core of the study of flexible robots. Due to the small selection of materials, single preparation method, and long fabrication time, in this study, a new method of gas-assisted extrusion (GAE) of elastic material round-tube for flexible robot body was proposed, and the numerical simulation of GAE was carried out with nonsilicone elastic material round-tube under different viscosities. The results showed that with the change of viscosity, the velocity, pressure drop, and shear rate of melt in all directions change accordingly. When the viscosity is too small or too large, it is easy to bring negative effects on the GAE process of elastic materials. TPE and TPU were completely plasticized in the GAE, and the surface of the extruded elastic products was smooth and straight, with full gloss. Therefore, in the preparation of the flexible robot body, nonsilicone elastic materials and GAE forming methods can be considered.

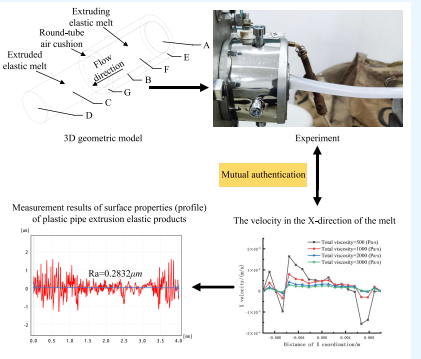

1. INTRODUCTION

In recent years, with the continuous advancements in bionics, soft intelligent materials, and advanced manufacturing technologies, the development of flexible robot inspired by soft-bodied animals in the natural world has emerged as a crucial research focus in the manufacturing field.[1] The flexible robot is constructed using soft materials and designed structurally to replicate the softness and adaptability found in biological organisms.[2,3] Its manufacturing usually involves the use of flexible, deformable, and controllable materials to ensure that the robot can achieve flexible morphology and movement.[4] The current ontology of flexible material manufacturing technology is limited by challenges such as single structure production, severe external interference, and high time costs, which makes its simulation and experimental research face many difficulties. Therefore, employing innovative design and synthesis methods to develop flexible robots holds immense practical application and socioeconomic value.

The Biology and Chemistry Laboratory of Harvard University produced a soft quadrupedal mobile robot whose body was made entirely of Ecoflex 0030 silicone material and did not contain any rigid skeletal structure.[5] Subsequently, the laboratory researchers used M4601 silicone material from Wacker Chemicals to manufacture an improved soft quadrupedal mobile robot body and embedded hollow glass microspheres to make a composite material with high-strength and low-density, to improve the load-bearing capacity of the airbag structure.[6] Panagiotis et al.[7,8] designed and manufactured a finger rehabilitation glove through silicone rubber elastic material, which conforms to the bending motion of different curvatures of the human finger movement range. Hao et al.[9] designed and produced a pneumatic soft hand claw with variable effective length by an injection molding process using soft material as raw material. Fionnuala et al.[10] used silicone rubber material to make a pipeline peristaltic robotic arm and realized different motion modes through different winding ways of fiber lines on the outer surface. Dong[11] designed a pneumatic soft body omnidirectional bending module using silicone material, Xu[12] used silicone material to design a new inflatable screw-actuated soft body pure torsion module, and Gong et al.[13] designed an underwater soft body robotic arm based on silicone material. At present, the body material of soft robots is mainly silica gel, and the experimental research using nonsilicone elastic material as the raw material is rarely involved. In this study, the nonsilicone elastic material is intended to be used as the body material of a flexible robot.

The mainstream manufacturing methods for flexible robot body include shape deposition,[14,15] nanopressure brushing,[16] intelligent microstructure synthesis,[17] and embedded molding.[18,19] The existing manufacturing methods[20,21] are mainly based on casting molding, with a longer production cycle and complex secondary processing. The manufacturing technology

Received: January 30, 2024
Revised: May 23, 2024
Accepted: May 27, 2024
Published: June 6, 2024

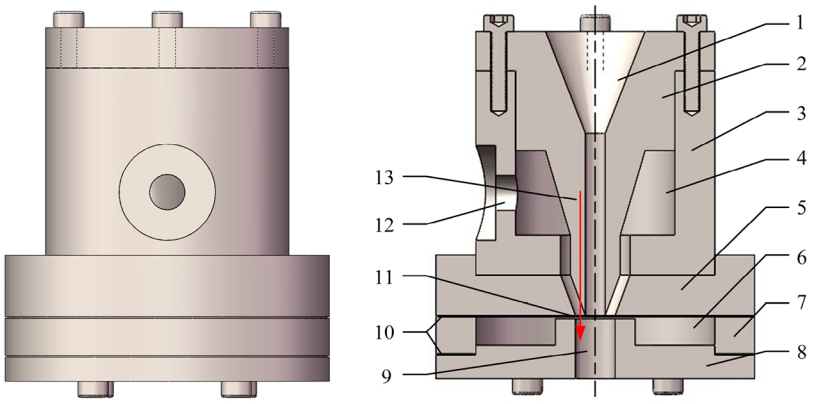

Figure 1. Experimental device and gas-assisted mold. (A) The overall structure of the die assembly, and (B) the sectional structure decomposition (where 1 is flow channel inlet, 2 is flow channel tube, 3 is gas chamber cavity, 4 is air chamber shell, 5 is gas-assisted transition section, 6 is gas chamber cavity, 7 is air chamber shell, 8 is bottom plate, 9 is gas-assisted section, 10 is gas gasket, 11 is gas cushion formed gap, 12 is holes on the outer shaft surface, and 13 is horizontal flow direction of gas).

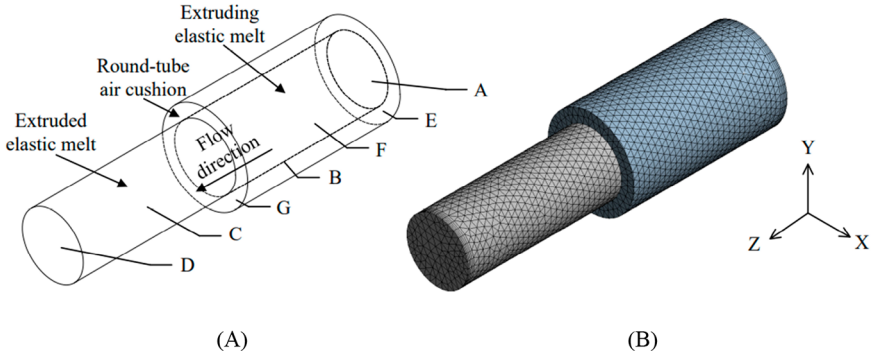

Figure 2. Melt round-tube geometric models. (A) The 3D geometric model sketch, and (B) the finite-element mesh of the geometric model.

based on gas-assisted extrusion (GAE) forming is mostly used for the processing and manufacturing of round tubes, square tubes, and irregular shapes, which has the advantages of high production efficiency and relatively simple secondary processing procedures. In this study, the GAE method[22−26] is intended to be used to manufacture the flexible robot body. The evolution of GAE forming technology dates back to the 1960s when it was predominantly used for extruding polyethylene foam plastics. It is a processing technique that expands or expands/contracts extruded plastics or rubber materials through high-temperature and high-pressure gas, allowing the expansion rate and shape of the material to be controlled. The current extrusion forming methods apply to viscoelastic melt, significantly improving the quality and efficiency of plastic extrusion products. Research on the application of elastic materials in GAE forming has proposed innovative simulation methods for extruding elastic materials.[27,28] These methods facilitate more precise predictions of the morphology and properties of the products.

The existing materials for flexible robot body cannot take into account the requirements of cost and production technology. This paper considered the application of GAE forming technology in the manufacture of flexible robot body. Due to the flexibility, scalability, and low viscosity of the flexible material, the nonsilicone elastomeric round-tube is used as the soft robot body, which can better adapt to the change of gas expansion or expansion/contraction in the GAE process, to obtain more accurate and controllable shapes and structure, and produce high-quality flexible robots.

2. MATERIALS AND METHODS

2.1. Materials and GAE Experimental Device. This paper used TPU[29] and TPE[30] (TPE TE-40A, TPU C 60 A HPM, BASF Co., Ltd.). Figure 1 depicts the experimental system for GAE in elastic material pipes that consists of three distinct sections. This encompasses a subsystem for extruding plastic pipes (comprising a single screw extruder, a cooling and sizing apparatus, and a traction device, among others), an enhanced GAE outlet die for elastic material pipes, and a gas-supported subsystem (including an air compressor and gas heating device). The extruder of SJ-30 was crafted by Wuhan Yiyang Plastic Co., Ltd., Shanghai Jialishi Machinery Co., Ltd. produced the air compressor, while Shanghai Laiheng Electric Appliance Co., Ltd. provided the gas heating apparatus. Figure 1 is the gas-assisted die employed in this study. Figure 1A is the comprehensive structural layout of the tube-type GAE die component, and Figure 1B is the schematic representation of the invention's sectional structural breakdown.

2.2. Experimental Methodology. Initially, the extruder was unlocked, followed by the execution of the TPE extrusion test. TPE particles were transferred from the hopper into the extruder barrel, with the die and polymer melt temperature at

https://doi.org/10.1021/acsomega.4c00967
ACS Omega 2024, 9, 25996−26003

160 °C (the first zone of the barrel was 145 °C, the second zone of the barrel was 155 °C, and the third zone of the barrel was 160 °C). A considerable duration was required to attain the predefined temperature. When the temperature was reached, the screw speed of the SJ-30 extruder was 4.5 r/min, and the speed of the tractor was 90 rpm to begin to extrude the melt. After the melt could be smoothly extruded, the gas heating equipment and the air compressor were worked, while the gas temperature was 160 °C and the gas pressure was 5000 Pa.[24] When the gas temperature was reached, the GAE experiment was started. After the extrusion experiment of TPE was completed, the hopper and barrel were emptied. The extrusion experiment of TPU was carried out, and the particles were put from the hopper into the extruder barrel. The die temperature and polymer melt temperature were set to 145 °C (the first zone of the barrel was 135 °C, the second zone of the barrel was 140 °C, and the third zone of the barrel was 140 °C), and the above operation was carried out.

3. NUMERICAL SIMULATION

3.1. Models. The geometric models of the melt round-tube are shown in Figure 2. The diameter of the cylinder is 20 mm, respectively, and the width of the thin gas circle is 8 mm, which is the stable gas layer formed between the periphery of the polymer melt and the inner wall of the die. The finite element mesh of the geometric model of the melt cylinder is shown in Figure 2B. To improve the computational accuracy, the number of meshes near the boundary and the gas layer is refined in the model. The mesh number is 6130.

3.2. Governing Equations. The governing equations of numerical simulation are as follows:

$$\nabla\cdot(\vec{v}) = 0 \tag{1}$$

$$\nabla\vec{p} - \nabla\cdot\vec{\tau} = 0 \tag{2}$$

where ∇ is the Hamilton operator, $\vec{v}$ is the melt's flow velocity, $\vec{p}$ is the melt's pressure, and $\vec{\tau}$ is the extra stress tensor.

In this study, Maxwell[29,30] is used as the constitutive equation of melt, as follows:

$$\begin{cases} \tau_1 + \lambda_{\tau_1}^{\nabla} = 2\eta_1 D \\ \tau_2 = 0 \end{cases} \tag{3}$$

In the formula, τ_1 is the viscoelastic part of the deviatoric stress tensor, τ_2 is the pure viscous part of the deviatoric stress tensor, $\lambda_{\tau_1}^{\nabla}$ is the upper adjoint derivative of the deviatoric stress tensor d, D is the deformation rate tensor, and η_1 is the viscosity corresponding to the viscoelastic part.

3.3. Boundary Conditions. (1) Inlet: In Figure 2A, the elastic melt is an incompressible non-Newtonian fluid. Section A is the inlet of the melt cylinders, and the melt inlet volume flow rate is 7.2×10^{-7} m^3/s. The gas is a compressible Newtonian fluid, where section E is the inlet of the gas. The pressure is 5000 Pa imposed on the inlet boundary of the gas.

(2) Walls: The turbulence effects of the gas are ignored by the wall surface of C and F, and the full slip boundary can be set to $v_n = v_s = 0$. v_n and v_s are the normal and tangential velocities.

(3) Interfaces: Section B is the interface between the melt and the gas, and the effects of inertia force and surface tension are ignored.

(4) Free surfaces: The free surface is section C, and there are no fluid passes, so the normal and tangential forces can be set to zero $f_n = f_s = 0$.

(5) Exit: The melt exit is section D, and the gas exit is section G. No drag force is applied at the exit $f_n = v_s = 0$.

3.4. Material Values. The material values of melt (elastic material)[31,32] and gas are given in Table 1.

Table 1. Material Values of Melt and Gas

parameters	total viscosity (Pa s)	ε
elastic material	500	0.1
	1000	0.1
	2000	0.1
	3000	0.1
gas	2.638×10^{-5}	0

4. RESULTS AND DISCUSSION

4.1. Simulation Influence and Results. The numerical simulation experiment is carried out to explore the influence of the viscosity of elastic materials on GAE. Because of the viscosity range of TPU,[31] TPE,[32] and other elastic materials, four different viscosities (500, 1000, 2000, and 3000 Pa s) are used for numerical simulation. The influence mechanism of melt on GAE molding of pipes is analyzed from the perspectives of velocity, pressure, and shear rate in all directions of melt.

4.1.1. Influence of Viscosity on the X-Velocity. Referring to Figure 2A, the midline in the width direction of the melt outlet was taken to calculate the numerical variation of the X-velocity. Subsequently, the X-velocity variation of the pipe flowing along the width direction at the outlet of the die was shown in Figure 3 for four different melt viscosities.

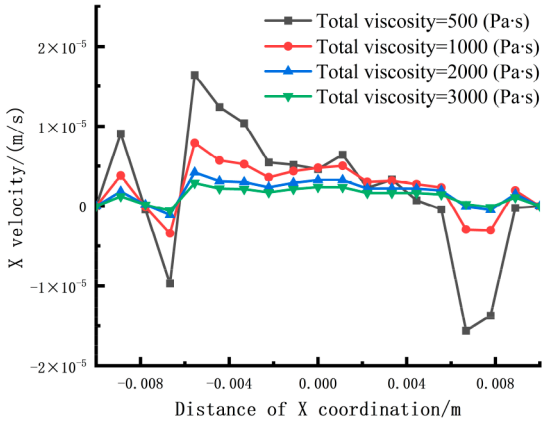

Figure 3. Variation of X-velocity along the width direction at the die exit under different viscosities.

It can be seen from Figure 3 that the X-velocity of the melt along the width direction changed at the die exit, while the X-velocity also decreased with the increase of the melt viscosity. For each melt viscosity, the X-velocity of the melt near the interface between the gas and the melt along the width direction was greater than the X-velocity of the internal melt. When the melt viscosity was 500 Pa s, the melt near the die wall produced a large negative flow velocity, and there was no expansion to the outer layer, but compared to the X-velocity at other viscosities, the maximum velocity 1.64×10^{-5} m/s was

https://doi.org/10.1021/acsomega.4c00967
ACS Omega 2024, 9, 25996−26003

larger. When the melt viscosity was greater than or equal to 1000 Pa s, the melt near the die wall would still produce a negative flow rate, but it was gradually decreasing. When the melt viscosity was 2000 or 3000 Pa s, the melt near the die wall would still produce a negative flow velocity, but the value of the flow velocity was small, and the two curves had a tendency to overlap. This indicates that when the viscosity increases to a certain extent, its influence on the flow rate in the *X*-direction will gradually weaken.

Therefore, for the melt at a certain flow rate, the *X*-direction velocity of the melt decreases with the increase of the viscosity of the melt when the viscosity is different under the gas-assisted effect, and the *X*-direction velocity near the interface between the melt and the gas is significantly higher than the *X*-direction velocity inside the melt. It shows that the gas has a positive drag effect on the melt and promotes the extrusion of the melt along the flow channel direction. When the elastic viscosity is less than a value, the gas is very likely to cause the melt to have a large fluctuation in the extrusion process, resulting in the phenomenon of off-mold expansion during pipe extrusion. According to the qualitative analysis, when the viscosity is too small, the difference between the *X*-velocity of the melt near the interface between the gas and the melt along the width direction and the *X*-velocity of the internal melt is too large, which may cause the melt to fluctuate during the extrusion process, resulting in rough surface swelling and even deformation. When the viscosity is too large, the influence of viscosity on the *X*-velocity along the width direction at the outlet of the die would gradually decrease until the *X*-velocity curve along the width direction at the outlet of the die coincides. Therefore, the appropriate viscosity plays a vital role in the extrusion process.

In addition, the numerical model of this paper is a pipe. The variation of *X*-velocity along the width direction is consistent with the change of *Y*-velocity along the height direction at the outlet of the die, so the influence of the variation of *Y*-velocity is not analyzed.

4.1.2. Influence of Viscosity on the Z-Velocity. Along the extrusion direction of the die flow channel, the midline of the interface between the melt and the gas was taken to calculate the numerical variation of the *Z*-velocity. Subsequently, the variation of *Z*-velocity when the pipe flows along the direction of the die channel is shown in Figure 4 for four different melt viscosities.

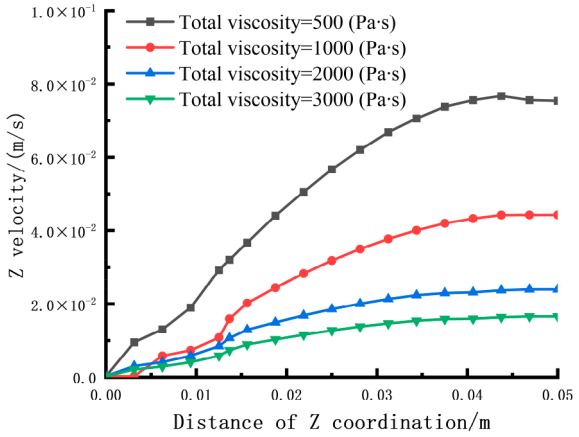

Figure 4. Variation of *Z*-velocity of round-tube in the die flow channel under different viscosities.

According to Figure 4, the *Z*-velocity of the melt increases with the increase of the distance of the melt in the die in the die channel. Because the gas velocity was much larger than the flow velocity, the gas had a dragging effect on the extrusion of the melt, which increased the *Z*-velocity along the extrusion direction continuously. With the increase of melt viscosity, the effect of gas on the melt was weaker. When the melt viscosity increased from 500 to 3000 Pa s, the maximum velocity of *Z* decreased from 7.67×10^{-2} to 1.66×10^{-2} m/s, which differs by 4.62 times. However, when the melt viscosity was greater than or equal to 2000 Pa s, the *Z*-direction velocity growth of the melt gradually slowed, and with the increase of the melt viscosity, the velocity growth was gentler. According to the qualitative analysis, this is due to the increase of melt viscosity, which weakens the drag effect of gas on the melt. The viscoelasticity of the melt played a role so that the velocity in the *Z*-direction was reduced to a certain extent. The gas introduced into the die had a positive drag effect on the melt compared to traditional extrusion. Reducing the melt viscosity would increase the extrusion speed of the melt in the *Z*-direction so that the melt would not stick to the die wall in a large probability, and the melt would be actively extruded. According to the qualitative analysis, the *Z*-speed increases faster in the die flow channel when the viscosity is too large. When the viscosity is too small, the influence of viscosity will gradually decrease the *Z*-velocity in the die channel until the *Z*-velocity curve coincides in the die channel. Therefore, the appropriate viscosity plays a vital role in the extrusion process.

4.1.3. Influence of Viscosity on the Melt Pressure. Along the extrusion direction of the die flow channel, the midline of the interface between the melt and the gas is taken to calculate the numerical variation of the pressure drop. Subsequently, the pressure drop distribution of the tube when extruded along the die flow channel is shown in Figure 5 for four different melt viscosities.

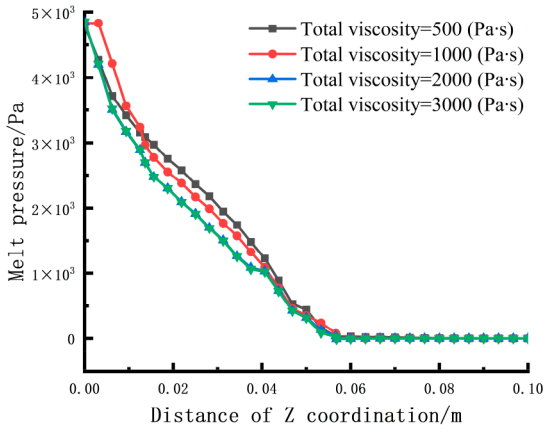

Figure 5. Variation of pressure of round-tube along the die runner under different viscosities.

As can be seen from Figure 5, the melt was subjected to a huge pushing force of the gas when contacting. The outer surface of the melt was subjected to the pressure of the gas into the melt, and a relatively large pressure drop would be generated between the melts. The pressure drop would increase rapidly near the entrance of the die. When the melt viscosity increased from 500 to 3000 Pa s, the overall pressure drop of the melt showed a downward trend, and the pressure drop curve with a viscosity of 500 Pa s is higher than other

https://doi.org/10.1021/acsomega.4c00967
ACS Omega 2024, 9, 25996−26003

pressure drop curves. The pressure drop curve with a viscosity of 1000 is lower than the pressure drop curve of 500 Pa s and higher than the pressure drop curves with viscosities of 2000 and 3000 Pa s. The pressure drop curves with viscosities of 2000 and 3000 Pa s overlapped on the whole, which indicates that the pressure drop would gradually decrease with the increase of viscosity. When the viscosity increases to a certain extent, the pressure drop would no longer decrease, and the slight decrease could be ignored. With the continuous exchange of energy and action between gas and melt, the internal and external pressure drop of melt reached equilibrium in a short time, which means the value of pressure drop decreased rapidly. Subsequently, the melt and gas reached a relatively stable equilibrium state near the exit of the die, and the pressure drop reached about zero. The pressure drop changed almost to zero after the exit die, which indicated that the extrusion process was relatively stable. According to the qualitative analysis, when the viscosity is too large, the influence of viscosity on the pressure drop along the die flow channel will gradually decrease until the pressure drop curve along the die flow channel coincides.

4.1.4. Influence of Viscosity on the Shear Rate. Along the extrusion direction of the die flow channel, the midline of the interface between the melt and the gas was taken to calculate the numerical variation of the shear rate. Subsequently, for the four different melt viscosities, the shear rate variation is shown in Figure 6 of the pipe during extrusion along the die channel on the surface.

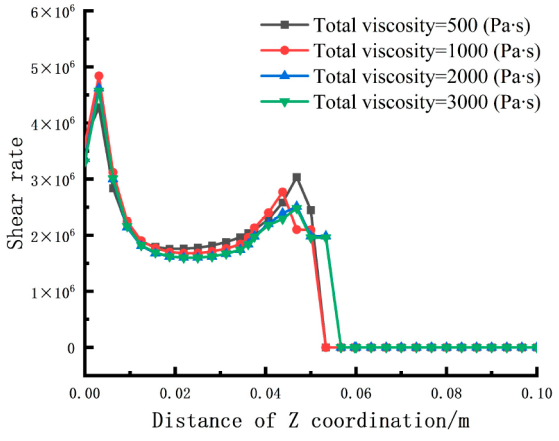

Figure 6. Shear rate variation on the surface of the round-tube along the flow channel of the die under different viscosities.

According to Figure 6, for each viscosity, the shear rate of the melt surface increased rapidly, and a peak appeared after the melt entered the die for some time. This was especially obvious when the melt viscosity was 2000 Pa s, and the maximum shear rate of the melt was 5.02×10^6 s^{-1}. The melt then gradually was adapted to the driving effect of high gas velocity, and the shear rate gradually decreased. Near the exit of the die, there was another peak of the shear rate. This was especially obvious when the melt viscosity was 500 Pa s, and the maximum shear rate of the melt was 3.03×10^6 s^{-1}. The shear rate decreased immediately when the melt went out of the die. The shear rate then decreased infinitely close to zero when the melt flowed in the extrusion direction.

For any viscosity, the shear rate of the melt on the surface decreased gradually along the flow direction, and it increased sharply near the die exit and then fell to about zero. When the melt extruded the die, the shear rate almost did not change, which was in a relatively balanced extrusion state. In the extrusion process, the interaction between the melt and the gas was continuous. Because the melt was viscoelastic, the elastic potential energy of the melt at the outlet of the die accumulated to a relatively high point. The shear effect was particularly obvious at the outlet, and then the melt quickly released internal energy to achieve a process of balance. According to the qualitative analysis, the viscosity of the melt is too small so the resistance inside the melt is weakened. The molecular motion will be more active, the time for the melt to recover energy will also be reduced, and the probability of deformation in the exit will be relatively large. When the viscosity of the melt is too high, the resistance inside the melt will increase, and the time for the melt to recover energy will also increase. When the viscosity increases to a certain extent, the influence on the shear rate becomes smaller in the extrusion process along the die flow channel.

4.2. Experimental Analysis and Results. Figure 7 is the state diagram of TPE and TPU pipe extrusion without and with the gas-assisted device after using the new die.

The state diagrams of TPU extruded with and without the gas-assisted device are shown in Figure 7A and B. When the TPU did not use the GAE device, there was no adhesion and water ripples during the extrusion process. The elastic products are seriously extruded and swelled, the surface is not smooth, and there are floccules. When the GAE device was used for the TPU, the formed air cushion was very stable during the extrusion process, and there was no adhesion, complete plasticization, and good melt fluidity. The elastic products have no extrusion swelling at the outlet, a smooth surface, and full gloss.

The state diagrams of TPE extruded with and without the gas-assisted device are shown in Figure 7C and D. When the TPE did not use the GAE device, there was no adhesion and a slight white crystal during the extrusion process. The elastic products are seriously extruded and swelled, the surface is not smooth, and there are floccules. When the GAE device was used for the TPE, the formed air cushion was very stable during the extrusion process, and there was no adhesion, complete plasticization, and good melt fluidity. The elastic products have no extrusion swelling at the outlet, a smooth surface, and full gloss.

The corresponding pipe extrusion samples without the use of the gas-assisted device extrusion and the use of gas-assisted device extrusion are shown in Figure 8. Whether it is TPE or TPU materials, the use of GAE of the corresponding pipe was much better than the use of GAE. The surface quality of the extruded product was relatively improved, the gloss was much better, and the surface was relatively smooth. Especially for TPU, the problem of extrudate swell and bulge of TPU was perfectly solved by GAE. By comparing the state of the extrudate, it was found that TPU has a better extrusion effect, including the gloss, smooth surface, and stretching effect.

To detect the influence of different process parameters on the surface of the pipe GAE samples, this study used a profile roughness measuring instrument (manufacturer: Sanfeng, Japan; model SV-C3200S4) to measure the contour shape of the product surface. The surface property (contour) measurement results of the elastic products are shown in Figure 9. The surface property (contour) measurement results of the TPU and TPE pipe extrusion samples were all guaranteed to be the

https://doi.org/10.1021/acsomega.4c00967
ACS Omega 2024, 9, 25996−26003

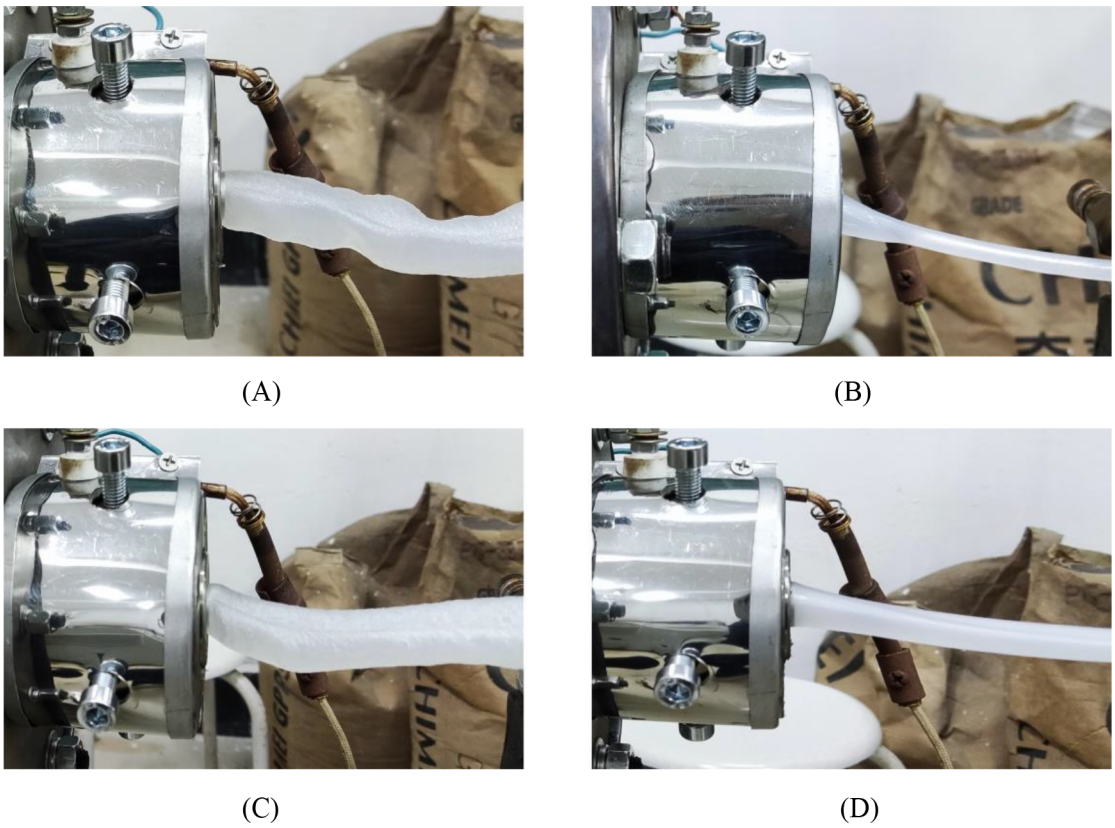

Figure 7. Extrusion state diagram of round-tube extrusion elastic products. (A) TPU without GAE. (B) TPU GAE. (C) TPE without GAE. (D) TPE GAE.

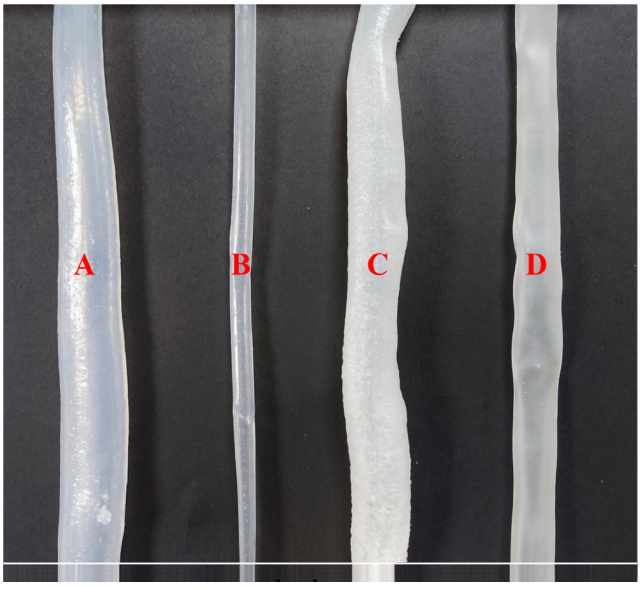

Figure 8. Extrusion elastic product of round-tube. (A) TPU without the GAE. (B) TPU with the GAE. (C) TPE without the GAE. (D) TPE with the GAE.

same *X*-rate, and the *Z*-rate was adjusted with the roughness change. Figure 9A shows the surface property (contour) measurement result of TPU extrusion without the gas-assisted device. The *X* and *Z* magnification of the product surface was 20 × 1000, the error magnification was ×100, and the roughness of the profile was 3.9122 μm. Figure 9B shows the surface property (contour) measurement result diagram of TPU extruded by the gas-assisted device. The *X* and *Z* magnification of the product surface was 20 × 10 000, the error magnification was ×100, and the roughness of the contour was 0.2832 μm. Figure 9C shows the surface property (contour) measurement result of TPE extrudate without the gas-assisted device. The *X* and *Z* magnification of the product surface was 20 × 2000, the error magnification was ×100, and the roughness of the contour was 2.1471 μm. Figure 9D shows the surface property (contour) measurement result diagram of TPE extruded by the gas-assisted device. The *X* and *Z* magnification of the product surface was 20 × 2000, the error magnification was ×100, and the roughness of the contour was 0.4661 μm. The above data indicate that the surface of the TPE and TPU samples using the gas-assisted devices is smooth and flat.

5. CONCLUSION

In this study, the numerical simulation was carried out on GAE of nonsilicone elastic material tubes with different viscosities to design a high-quality flexible robot body. The simulation results show that the velocity, pressure drop, and shear rate of the melt in all directions would change with the variation of viscosity. When the viscosity was too small, the difference of extrusion speed inside the melt was too large, the melt was easy to fluctuate during the extrusion process, and the deformation of the melt was large. However, when the viscosity was too large, the melt was prone to adhesion during the extrusion process, which had a negative impact. Subsequently, the extrusion experiment of the elastic material was carried out. The experiment showed that the TPE and TPU formed by GAE were completely plasticized during the extrusion process,

https://doi.org/10.1021/acsomega.4c00967
ACS Omega 2024, 9, 25996−26003

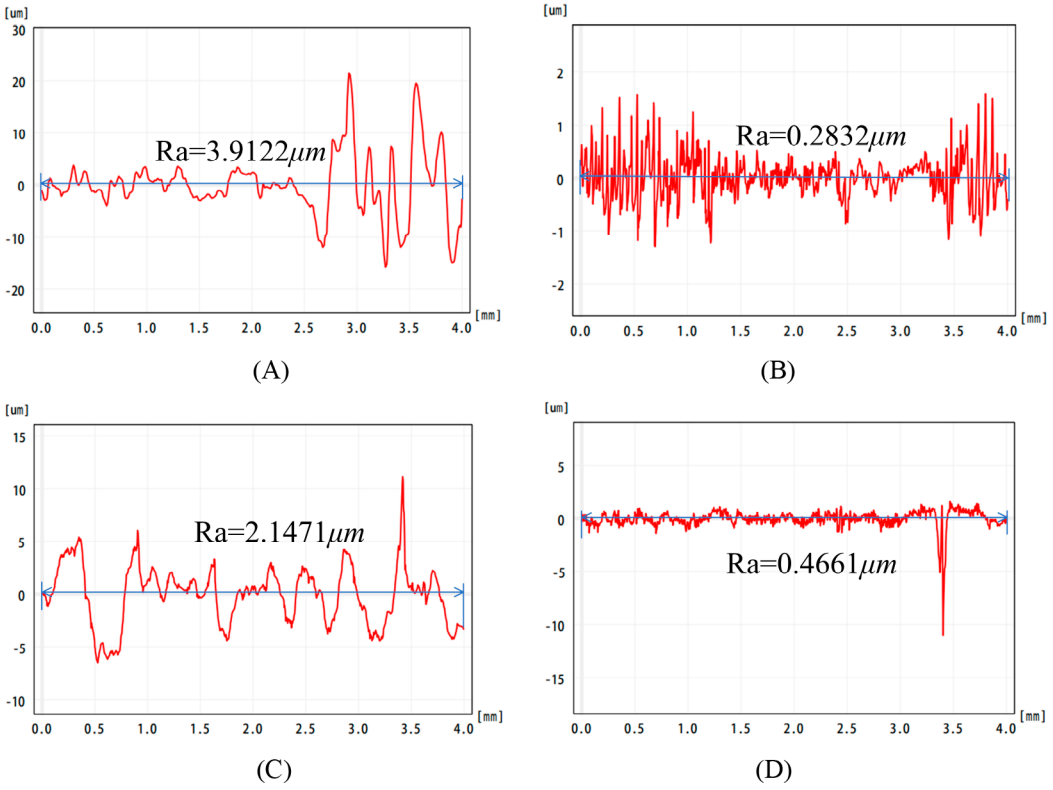

Figure 9. Measurement results of the surface properties (profile) of round-tube extrusion elastic products. (A) TPU without the GAE. (B) TPU with the GAE. (C) TPE without the GAE. (D) TPE with the GAE.

the melt fluidity was good, the formed air cushion was stable, and the surface of the extruded elastic product was smooth and straight, with full gloss. Therefore, when preparing the flexible robot body, nonsilicone elastic materials and GAE molding methods could be considered, and the gloss, plasticizing degree, and melt fluidity of the elastic products have more advantages.

■ ASSOCIATED CONTENT

Data Availability Statement

The data that support the findings of this study are available from the corresponding author upon reasonable request.

■ AUTHOR INFORMATION

Corresponding Authors

Songtao Wang − *School of Mechanical Engineering, Nanchang Institute of Technology, Nanchang, Jiangxi 330099, China*; Email: santeer@foxmail.com

Liling Zhang − *School of Mechanical Engineering, Nanchang Institute of Technology, Nanchang, Jiangxi 330099, China*; Email: zlljdx@163.com

Authors

Shiyu Jiang − *School of Mechanical Engineering, Nanchang Institute of Technology, Nanchang, Jiangxi 330099, China; Engineering Research Center of Railway Environment Vibration and Noise Nanchang, East China Jiao Tong University, Nanchang, Jiangxi 330013, China*; orcid.org/0000-0003-4305-6277

Yimeng Yu − *School of Mechanical Engineering, Nanchang Institute of Technology, Nanchang, Jiangxi 330099, China*

Zhong Yu − *School of Physics and Electronic Information Shangrao, Shangrao Normal University, Shangrao, Jiangxi 334001, China*

Zhi Shen − *School of Mechanical Engineering, Nanchang Institute of Technology, Nanchang, Jiangxi 330099, China*

Complete contact information is available at: https://pubs.acs.org/10.1021/acsomega.4c00967

Notes

The authors declare no competing financial interest.

■ ACKNOWLEDGMENTS

This work was supported by the National Natural Science Foundation of China (NSFC, no. 52265002), the Jiangxi Natural Science Foundation (no. 20232BAB204042), the Teaching Reform Program of Jiangxi Colleges and Universities (no. JXJG22186), Science and Technology of the Education Department of Jiangxi Province (nos. GJJ2201517 and GJJ2201815), the Nanchang Institute of Technology school-level curriculum ideological and political project (2023JG019), and the Nanchang Institute of Technology to introduce a doctoral research project (no. 2022kyqd023).

■ REFERENCES

(1) Niiyama, R. Soft Actuation and Compliant Mechanisms in Humanoid Robots. *Current Robotics Reports* **2022**, *3* (3), 111−117.

(2) Lin, Y.; Siddall, R.; Schwab, F.; et al. Modeling and control of a soft robotic fish with integrated soft sensing. *Advanced Intelligent Systems* **2023**, *5* (4), 2000244.

(3) He, S. Y.; Sun, L. L.; Xu, Y. W.; et al. A Modeling and Data-driven Control Framework for Rigid-soft Hybrid Robot with Visual Servoing. *IEEE Robotics and Automation Letters* **2023**, *8* (11), 7281−7288.

https://doi.org/10.1021/acsomega.4c00967
ACS Omega 2024, 9, 25996−26003

(4) Yu, Z.; Peiyu, H.; Bo, Y.; Zhibin, Y.; Dongjie, L.; Guoqi, D.; et al. Design and Motion Simulation of a Soft Robot for Crawling in Pipes. *Applied Bionics and Biomechanics* **2023**, *2023* (1), 5334604.
(5) Shepherd, R. F.; Ilievski, F.; Choi, W.; et al. Multigait soft robot[J]. *Proc. Natl. Acad. Sci. U. S. A.* **2011**, *108* (51), 20400−20403.
(6) Tolley, M. T.; Shepherd, R. F.; Mosadegh, B.; et al. A resilient untethered soft robot[J]. *Soft Robot* **2014**, *1* (3), 213−223.
(7) Polygerinos, P.; Lyne, S.; Wang, Z.; et al. Towards a soft pneumatic glove for hand rehabilitation. *IEEE/RSJ International Conference on Intelligent Robots and Systems*; IEEE, 2014; pp 1512−1517.
(8) Polygerinos, P.; Wang, Z.; Galloway, K. C.; et al. Soft robotic glove for combined assistance and athome rehabilitation[J]. *Robotics & Autonomous Systems* **2015**, *73* (C), 135−143.
(9) Hao, Y.; Gong, Z.; Xie, Z.; et al. Universal soft pneumatic robotic gripper with variable effective length. *Chinese Control Conference*; IEEE, 2016; pp 6109−6114.
(10) Connolly, F.; Polygerinos, P.; Walsh, C. J.; et al. Mechanical programming of soft actuators by varying fiber angle. *Soft Robot.* **2015**, *2* (1), 26−32.
(11) Dong, H. B. Research on key technologies of a pneumatic soft omnidirectional bending module. Harbin Institute of Technology, 2016.
(12) Xu, B. B. Research on pneumatic spiral driven pure torsional soft robotic module. Harbin Institute of Technology, 2017.
(13) Zheyuan, G.; Jiahui, C.; Kainan, H., Tianmiao, L. W. An inverse kinematics method of a softrobotic arm with three-dimensional locomotion for underwater manipulation. *IEEE International Conference on Soft Robotics*; IEEE, 2018; pp 516−521.
(14) Yilmaz, O.; Ugla, A. Development of a cold wire-feed additive layer manufacturing system using shaped metal deposition method[J]. *Journal of Mechanical Science and Technology* **2017**, *31* (4), 1611−1620.
(15) Liu, J.; Ma, Y.; Qureshi, A. J.; Ahmad, R. Light-weight shape and topology optimization with hybrid deposition path planning for FDM parts[J]. *International Journal of Advanced Manufacturing Technology* **2018**, *97* (1), 1123−1135.
(16) Ji, L.; Sorono, D. V.; Chait, C.; Chai, Tc; Zhang, X. 3-D numerical and experimental investigations on compression molding in multichip embedded wafer level packaging[J]. *IEEE Transactions on components, packaging and manufacturing technology* **2013**, *3* (4), 678−687.
(17) Mohammadi, Y.; Saeb, M. R.; Penlidis, A.; Jabbari, E.; Zinck, P.; Stadler, F.; Matyjaszewski, K. Intelligent Monte Carlo: a new paradigm for inverse polymerization engineering. *Macromol. Theory Simul.* **2018**, *27* (3), 1700106.
(18) Bavafaye Haghighi, E.; Rahmati, M.; Palm, G.; Shiry Ghidary, S. Learning Inductive Riemannian Manifold in Abstract Form by Modeling Embedded Dynamical System. *Informatica* **2014**, *25* (3), 361−384.
(19) Rauber, T.; Rünger, G. Parallel execution of embedded and iterated Runge−Kutta methods[J]. *Concurrency: Practice and Experience* **1999**, *11* (7), 367−385.
(20) Haque, F. Z.; Ali, V.; Husain, M. Synthesis and spectroscopic characterization of Nile Blue doped silica gel rods. *Optik* **2013**, *124* (20), 4287−4291.
(21) Haque, F. Z.; Husain, M. Synthesis and spectroscopic characterization of coumarin 440 dye doped silica gel rods[J]. *Optik* **2014**, *125* (10), 2308−2312.
(22) Liu, T. K.; Huang, X. Y.; Luo, C.; et al. The Formation Mechanism of the Double Gas Layer in Gas-Assisted Extrusion and Its Influence on Plastic Micro-Tube Formation[J]. *Polymers* **2020**, *12* (2), 355.
(23) Jiang, S. Y.; Liu, H. S.; Huang, X. Y.; et al. Numerical and experimental studies on the effect of thickness difference between up and down gas layers on sheet polymer gas-assisted extrusion forming[J]. *Polym. Eng. Sci.* **2020**, *60* (10), 2470−2486.
(24) Jiang, S. Y.; Liu, H. S.; Huang, X. Y.; et al. Improved die assembly for gas-assisted sheet extrusion using different up and down gas layer thicknesses[J]. *Polym. Eng. Sci.* **2021**, *61* (5), 1546−1558.
(25) Jiang, S. Y.; Liu, H. S.; Yu, Z.; et al. Comparative analysis of gas-assisted extrusion of polypropylene sheet based on two types of gas intake[J]. *Journal of Polymer Engineering* **2023**, *43* (4), 386−398.
(26) Jiang, S. Y.; Liu, H. S.; Yu, Z.; et al. Research on Improved Gas-Assisted Extrusion of Plastic Sheets Based on Time-Temperature Equivalence Principle[J]. *Polym. Eng. Sci.* **2023**, *63* (7), 2093−2102.
(27) Li, X. Y. A kind of silicone rubber elastic material and its preparation method. CN202111245022.0, 2022.
(28) Gu, Y.; Lin, P. C.; Zhang, J. K. Preparation and Afterglow Mechanoluminescent Property of ZrO2:Ti^{4+}/PDMS Composite Elastic Material. *J. Chin. Ceram. Soc.* **2022**, *50* (12), 7.
(29) Bistafa, S. R. The Navier−Stokes equation from Maxwell's Theory of Gases[J]. *Journal of the Brazilian Society of Mechanical Sciences and Engineering* **2018**, *40* (1), 1−10.
(30) Biswas, A.; Prasad, V. V.; Raz, O. Mpemba effect in driven granular Maxwell gases. *Phys. Rev. E* **2020**, *102* (1), 012906.
(31) Choi, E. Y.; Kim, S. W.; Lee, J. Y. Characteristics of Polyurethane Composites Containing Polyurethane Grafted Multi-walled Carbon Nanotubes[J]. *POLYMER-KOREA* **2017**, *41* (3), 490−494.
(32) Jiao, Y.; Yang, R.; Luo, Y. Fulgide derivative-based solid-state reversible fluorescent switches for advanced optical memory[J]. *CCS Chemistry* **2022**, *4* (1), 132−140.

https://doi.org/10.1021/acsomega.4c00967
ACS Omega 2024, 9, 25996−26003